

NOCTA: Non-Greedy Objective Cost-Tradeoff Acquisition for Longitudinal Data

Dzung Dinh ^{*1} Boqi Chen ^{*1} Yunni Qu ¹ Marc Niethammer ² Junier Oliva ¹

Abstract

In many critical domains, features are not freely available at inference time: each measurement may come with a cost of time, money, and risk. Longitudinal prediction further complicates this setting because both features and labels evolve over time, and missing measurements at earlier timepoints may become permanently unavailable. We propose NOCTA, a Non-Greedy Objective Cost-Tradeoff Acquisition framework that sequentially acquires the most informative features at inference time while accounting for both temporal dynamics and acquisition cost. NOCTA is driven by a novel objective, NOCT, which evaluates a candidate set of future feature-time acquisitions by its expected predictive loss together with its acquisition cost. Since NOCT depends on unobserved future trajectories at inference time, we develop *two complementary* estimators: (i) NOCT-Contrastive, which learns an embedding of partial observations utilizing the induced distribution over future acquisitions, and (ii) NOCT-Amortized, which directly predicts NOCT for candidate plans with a neural network. Experiments on synthetic and real-world medical datasets demonstrate that both NOCTA estimators outperform existing baselines, achieving higher accuracy at lower acquisition costs.

1. Introduction

In many real-world scenarios, *the inference-time acquisition of information is a critical decision*. For example, in clinical settings (a driving application for this work), diagnostic decisions often rely on sequentially gathering information such as lab tests or imaging. Each type of data acquisition comes at a cost of time, financial expense, or risk to

^{*}Equal contribution ¹Department of Computer Science, UNC Chapel Hill ²Department of Computer Science and Engineering, University of California San Diego. Correspondence to: Dzung Dinh <ddinh@cs.unc.edu>.

Preprint. February 10, 2026.

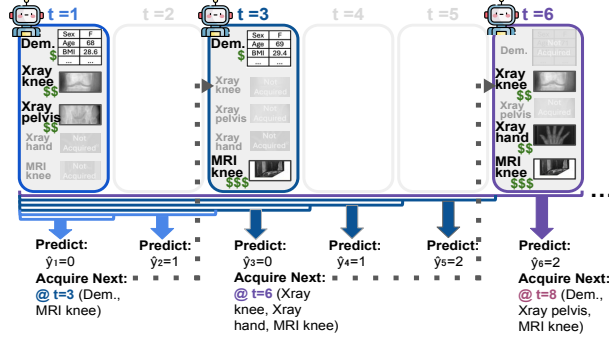


Figure 1. Illustration of clinical longitudinal AFA. At the current visit, an autonomous agent reviews previously collected and newly acquired data, predicts the patient’s current status, and recommends a subset of examinations for a determined future timepoint. This process repeats until the agent recommends no further acquisition.

the patient. In contrast, standard supervised machine learning pipelines typically assume that *all* features are freely available at inference.

In this work, we focus on *longitudinal* Active Feature Acquisition (LAFA) (Saar-Tsechansky et al., 2009; Kossen et al., 2023), where, during inference, a model is responsible for (i) sequentially deciding *which features* to acquire and at *what time*, balancing their utility against acquisition costs, and (ii) *making predictions* with the partially observed features it has chosen to acquire. In this setting, leveraging the temporal context is crucial for both selecting valuable feature acquisitions and making accurate predictions. Fig. 1 illustrates an example of LAFA by an autonomous agent in a clinical scenario. At the current visit, the agent (1) reviews previously collected data alongside any measurement acquired at the current visit, (2) predicts the patient’s current status \hat{y}_t , and (3) decides when to schedule the next visit and which tests to acquire then (accounting for measurements’ acquisition costs). Practical constraints such as time, cost, and resource limitations necessitate a judicious selection. Between visits, the agent continues to forecast the disease progression utilizing the previous acquisitions.

This longitudinal AFA setting presents several challenges, including: deciding which features to acquire at each visit, facilitating early predictions for timely interventions, and ac-

counting for temporal settings where missed acquisitions at earlier time points are permanently inaccessible. Although previous work has explored various approaches for longitudinal AFA, some methods (Kossen et al., 2023) make a single prediction across all time points, neglecting dynamic predictions, which are critical in clinical settings to detect deterioration early and adjust treatment plans (Qin et al., 2024). Furthermore, recent reinforcement learning (RL)-based methods (Qin et al., 2024; Nguyen et al., 2024) can be difficult to optimize in practice, while greedy strategies (Gadgil et al., 2024) risk suboptimal decisions because they focus on short-term gain and may skip early measurements that later prove critical but cannot be reacquired. This motivates non-greedy methods that are practical to train and deploy.

Contributions We propose NOCTA (Non-Greedy Objective Cost-Tradeoff Acquisition), a non-greedy framework for longitudinal AFA that explicitly plans over future acquisitions without training an RL policy. First, we introduce NOCT, the longitudinal objective underlying NOCTA that balances prediction accuracy against the cost of acquiring features. Second, we develop two practical estimators for scoring candidate acquisition plans under NOCT: (1) NOCT-Contrastive, an embedding-based estimator that learns a representation for scoring candidate plans from partial observations, trained with a contrastive objective, and (2) NOCT-Amortized, a neural estimator that directly predicts the NOCT value of a candidate plan from the current available information. Third, we present the NOCTA planning algorithm that uses these estimators to select acquisitions at inference time. Fourth, we provide theoretical analyses that support NOCT and our planning strategies. Fifth, across synthetic and real-world medical datasets, we show that NOCTA achieves consistent improvements over state-of-the-art (SOTA) baselines.

2. Related Work

Active Feature Acquisition Prior works in AFA (Saar-Tsechansky et al., 2009; Sheng and Ling, 2006) study the trade-off between prediction and feature acquisition cost in a non-longitudinal context. Recent works (Shim et al., 2018; Yin et al., 2020; Janisch et al., 2020) frame AFA as an RL problem; however, they are challenging to train in practice due to the complicated state and action space with dynamically evolving dimensions. Other works (Li and Oliva, 2021) use surrogate generative models, which model multidimensional distributions, or employ greedy policies that ignore joint informativeness (some features are only informative in combination) (Covert et al., 2023; Ma et al., 2019; Gong et al., 2019). To overcome these issues, Valancius et al. (2024) employ a non-parametric oracle-based method, and Ghosh and Lan (2023) learn a differentiable acquisition policy by jointly optimizing selection and prediction models

through end-to-end training. However, these works address AFA in a non-temporal context, whereas many real-world tasks require sequential decisions over time, motivating the need for *longitudinal* AFA.

Longitudinal Active Feature Acquisition Longitudinal AFA extends the standard AFA to include the temporal dimension. In this setting, a policy must account for temporal constraints where past time points can no longer be accessed. As a result, a policy must decide which features to acquire and determine the optimal timing for each acquisition. For instance, Zois and Mitra (2017) derive dynamic-programming and low-complexity myopic policies for finite-state Markov chains, ASAC (Yoon et al., 2019) uses an actor-critic approach to jointly train a feature selection and a prediction network. Additionally, Nguyen et al. (2024) use RL to optimize acquisition timing, but acquire all available features at the selected time point. Recently, Qin et al. (2024) prioritize timely detection by allowing flexible follow-up intervals in continuous-time settings, ensuring that predictions are timely and accurate. However, RL-based approaches can be challenging to train due to issues such as sparse rewards, high-dimensional observation spaces, and complex temporal dependencies (Li and Oliva, 2021). Rather than relying on RL to learn a policy, our proposed approach, NOCTA, explicitly plans by scoring future candidate acquisitions using either NOCT-Contrastive or NOCT-Amortized.

3. Methodology

Notation We consider longitudinal AFA over a dataset $\mathcal{D} = \{(x_i, y_i)\}_{i=1}^N$ of N instances (e.g., patients). For each instance i , the covariates form a sequence of length L : $x_i = \{x_{i,t}\}_{t=1}^L$, where $t \in \{1, \dots, L\}$ indexes the time step. At each time step t , $x_{i,t} \in \mathbb{R}^M$ contains M (costly) feature measurements, but the policy may only acquire a subset at each visit¹. We study a classification task with per-timepoint labels $y_{i,t} \in \{1, 2, \dots, C\}$, where C represents the number of classes. Following Qin et al. (2024); Yoon et al. (2019), each feature m has a time-invariant² cost c^m . Finally, we use colon notation for subsequences; for example, $x_{1:t} = (x_1, \dots, x_t)$ denotes measurements from timepoints 1 to t (inclusive).

3.1. Longitudinal AFA modeled as an MDP

Longitudinal AFA can be formulated as a Markov Decision Process (MDP). The state $s_t = (x_o, o, t)$, where x_o denotes the (partial) observations before time t and

¹NOCTA also supports multi-modal acquisitions where each modality yields a vector; this can be modeled by replacing scalar features with modality-specific vectors.

²NOCTA easily extends to time-varying costs by replacing c^m with $c^{m,t}$ (cost of modality m at time t).

$o \subseteq \{(m, t') \mid m \in \{1, \dots, M\}, t' \in \{1, \dots, t-1\}\}$ records which features were acquired. We suppose access to a pre-trained arbitrary conditioning classifier \hat{y} (Shim et al., 2018; Li and Oliva, 2021) that can predict the label at any target timepoint k with the current information, i.e., $\hat{y}_k(x_o)$. Note that the same input information can be used to predict at other time points, $\hat{y}_{k'}(x_o)$ (where forward prediction corresponds to when feature observations in o occur before k'). The action space is $a \in \{a_{t'}\}_{t'=t}^L \cup \{\emptyset\}$, where $a_{t'} \in \{0, 1\}^M$ indicates which of the M features to acquire at time t' , or, when $a = \emptyset$, to terminate and predict all remaining timepoints. For a non-terminal action, the transition is $(x_o, o, t) \rightarrow (x_{o \cup a_{t'}}, o \cup a_{t'}, t'+1)$, where (for notational simplicity) $o \cup a_{t'}$ denotes the union of the previous acquisitions and tuples of features at time t' in $a_{t'}$. Since this implies that we are not acquiring any information until time t' , the reward is the negative cross-entropy (CE) loss of making predictions up to t' (i.e., $\hat{y}_t, \dots, \hat{y}_{t'-1}$) with previous information (x_o) and respective negative CE loss and cost of acquiring new features at time t' : $-\sum_{k=t}^{t'-1} \text{CE}(\hat{y}_k(x_o), y_k) - \text{CE}(\hat{y}_{t'}(x_{o \cup a_{t'}}), y_{t'}) - \alpha \sum_{m=1}^M a_{t',m} c^m$, where α is an *application-specific* accuracy-cost tradeoff parameter; certain applications allow a higher cost (i.e., lower α) and some are more cost-restricted (i.e., high α). When terminated ($a = \emptyset$) at timepoint t , we are not acquiring any additional information for the remaining timepoints, thus the reward is $-\sum_{k=t}^L \text{CE}(\hat{y}_k(x_o), y_k)$, which represents the negative cross-entropy loss accumulated from t to L using the current information at hand. We denote our policy as $\pi(x_o, o, t)$, which selects actions to maximize the expected cumulative rewards through L .

Longitudinal AFA MDP Challenges Modeling longitudinal AFA as an MDP introduces several difficulties: (1) *a large and complicated action space*, since one requires decisions on when to acquire and which features to acquire; (2) *a complicated state space*, as it evolves dynamically over the combinatorial acquisitions as new features are captured over time; and (3) *a credit assignment problem*, since acquisitions are awarded at an aggregate level, it is hard to disentangle exactly which of the acquired features were most responsible for prediction rewards (Li and Oliva, 2021). Despite these challenges, prior work (Qin et al., 2024; Yoon et al., 2019; Kossen et al., 2023; Nguyen et al., 2024) often relies on RL for longitudinal AFA. In contrast, we propose NOCTA, an RL-free approach that not only provides a theoretical lower bound on the optimal longitudinal AFA MDP value (see Appx. A.4), but also empirically outperforms RL-based baselines.

3.2. Non-Greedy Objective Cost-Tradeoff

We now introduce NOCTA through a novel longitudinal objective that provides a provable (see be-

low) proxy for the MDP value of states. Let $\mathcal{V}_{>t} = \{(m, t') \mid m \in \{1, \dots, M\}, t' \in \{t+1, \dots, L\}\}$ represent the set of candidate feature-time pairs that are still available to acquire after time t . At a partially observed state (x_o, o, t) , we have two options: (1) *choose an acquisition plan* $v \subseteq \mathcal{V}_{>t}$ (which specifies what to acquire in the future), or (2) *terminate acquisition* (i.e., $v = \emptyset$) and make predictions for the remaining timepoints using only the currently observed information x_o . The **non-greedy objective cost-tradeoff** (NOCT) determines the tradeoff of an acquisition plan of additional features $v \subseteq \mathcal{V}_{>t}$ for a current partially known instance of x_o (o containing features from the past, $\leq t$):

$$\text{NOCT}(x_o, o, v) \equiv \mathbb{E}_{y_{t+1:L}, x_v | x_o} [\ell(x_o \cup x_v, y, t)] + \alpha \sum_{(m, t') \in v} c^m, \quad (1)$$

where $\ell(x_o \cup x_v, y, t) \equiv \sum_{k=t+1}^L \text{CE}(\hat{y}_k(x_o \cup x_{v_{t+1:k}}), y_k)$ is the accumulated cross-entropy loss from $t+1$ to L when acquiring the future feature-time pairs specified by v . Here, $x_{v_{t+1:k}}$ denotes the subset of acquired features in v whose time indices lie in $\{t+1, \dots, k\}$, i.e., the features that would be available by time k under plan v , given the currently observed information x_o . Using trajectories $(x_v, y_{t+1:L})$ in the training set \mathcal{D} , the expectation in Eq. (1) can be directly estimated within an instance during training. At inference time, x_v is unobserved, so we approximate Eq. (1) using the estimator in Sec. 3.4 and Sec. 3.5. Intuitively, Eq. (1) looks ahead at how acquiring a new set of feature-time pairs in $\mathcal{V}_{>t}$ is anticipated to reduce the classification loss from $t+1$ to L , while penalizing the acquisition cost (see Fig. 2(a)). For simplicity, we refer to feature-time pairs as “features”.

3.3. NOCT Acquisition (NOCTA)

At time t , one may use NOCT (Eq. (1)) to indicate the best anticipated future acquisition plan given the current information, $u(x_o, o)$:

$$u(x_o, o) \equiv \underset{v \subseteq \mathcal{V}_{>t}}{\text{argmin}} \text{NOCT}(x_o, o, v); \quad (2)$$

i.e., plan according to the anticipated cost tradeoff of obtaining future features for future prediction targets. In fact, we can show that the NOCTA criterion in Eq. (2) is a principled proxy value for partially acquired states:

Theorem 3.1. (Informal) –NOCT lower bounds the value of the optimal longitudinal AFA MDP policy

In other words, acquiring by following the plan selected in Eq. (2) serves as an approximation to the optimal longitudinal AFA MDP policy (full proof in Appx. A.4).

Acquisition Algorithm When Eq. (2) returns $u(x_o, o) = \emptyset$, it indicates that the potential loss improvement does not

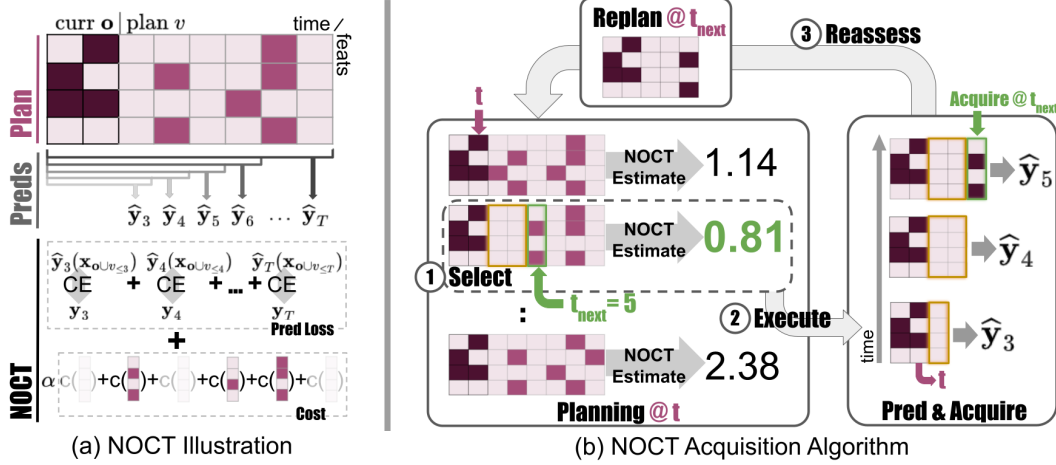


Figure 2. Overview of NOCTA. **(a) NOCT evaluation of plan.** Given partially observed state (x_o, o, t) , a candidate plan $v \subseteq \mathcal{V}_{>t}$ (a feature \times time matrix) is evaluated by the tradeoff of (i) the expected accumulated predictive cross-entropy (CE) loss for future acquisitions from $t+1$ to L and (ii) the acquisition cost of selected future acquisitions (i.e., $\alpha \sum_{(m, t') \in v} c^m$). Under plan v , the prediction at future time k only uses acquisitions up to time k (i.e., $\hat{y}_k(x_{o \cup v \leq k})$). **(b) Acquisition algorithm.** At state (x_o, o, t) , the NOCTA algorithm evaluates candidate plans $v \subseteq \mathcal{V}_{>t}$ with a NOCT estimator. (1) We select the best plan, \hat{u} , according to the NOCT estimates. (2) We execute the selected plan up to its next acquisition (i.e., $t_{\text{next}} \equiv \min t' : (m, t') \in \hat{u}$) by acquiring $a_{t_{\text{next}}} \equiv \{(m, t_{\text{next}}) \in \hat{u}\}$. Predictions are made at every timepoint; e.g., as illustrated, with $t=2$ and $t_{\text{next}}=5$, NOCTA predicts at $t=3, 4$ using current information (i.e., $\hat{y}_3(x_o), \hat{y}_4(x_o)$) and predicts at $t_{\text{next}}=5$ using newly observed features (i.e., $\hat{y}_5(x_{o \cup a_{t_{\text{next}}}})$). (3) We reassess with $x_o \equiv x_{o \cup a_{t_{\text{next}}}}$ and $t \equiv t_{\text{next}}$, repeating until the selected plan is empty ($\hat{u} = \emptyset$) or when we reach the final time step ($t=L$).

justify the cost of acquiring further future features, so we stop acquiring and predict for all subsequent time points using the currently observed features x_o . Otherwise, if a non-empty plan $u(x_o, o) = v \subseteq \mathcal{V}_{>t}$ is selected, it indicates that, given x_o , the set $u(x_o, o)$ yields the best trade-off for future predictions. Carrying out the selected plan $u(x_o, o)$, implies that the next acquisition occurs at $t_{\text{next}} \equiv \min\{t' \mid (m, t') \in u(x_o, o)\}$, the earliest timepoint in the plan. This implies that all the predictions until t_{next} are to be done with the current information, $\hat{y}_{t+1}(x_o), \dots, \hat{y}_{t_{\text{next}}-1}(x_o)$, and the prediction at t_{next} includes the planned features at t_{next} , $a_{t_{\text{next}}} \equiv \{(m, t_{\text{next}}) \mid (m, t_{\text{next}}) \in u(x_o, o)\}$, $\hat{y}_{t_{\text{next}}}(x_{o \cup a_{t_{\text{next}}}})$. We may similarly continue with acquisitions in $u(x_o, o)$ for timepoints after t_{next} . However, a more dynamic strategy is to incorporate the newly acquired feature values to reassess (update) the best anticipated plan. That is, compute $u(x_{o \cup a_{t_{\text{next}}}}, o \cup a_{t_{\text{next}}})$ using $\mathcal{V}_{t_{\text{next}}}$, for further acquisitions after t_{next} (see Fig. 2(b)).

Proposition 3.2. *(Informal) Replanning after each acquisition is never worse (in terms of the NOCT objective) than committing to the original plan's remainder (full proof in Appx. A.5).*

Note that $u(x_{o \cup a_{t_{\text{next}}}}, o \cup a_{t_{\text{next}}})$ is a dominating strategy to simply proceeding with $u(x_o, o)$ since: 1) it incorporates additional information, which provides more context (using values in $a_{t_{\text{next}}}$) for the anticipated utility of further acquisitions; 2) the search for $u(x_{o \cup a_{t_{\text{next}}}}, o \cup a_{t_{\text{next}}})$ includes the original plan for further acquisition from $u(x_o, o)$, so it

may stick to the previous plan if it is still anticipated to be optimal in light of new values. Intuitively, this dynamic strategy avoids a stubborn approach that does not update its acquisition plans in light of additional information. The acquisition process of NOCTA is detailed in Alg. 1.

Algorithm 1 NOCTA

Require: Number of features M , number of time steps L , cost for feature m as c^m , estimator \hat{y}_k .

```

1: Initialize: predictions  $\leftarrow []$ ; terminate  $\leftarrow$  false;
    $t \leftarrow 0$ ;  $o \leftarrow \emptyset$ 
2: while not terminate do
3:    $\mathcal{V}_{>t} \leftarrow \{(m, t') \mid m \in \{1, \dots, M\}, t' \in \{t+1, \dots, L\}\}$ 
4:    $\hat{u}(x_o, o) \approx \underset{v \subseteq \mathcal{V}_{>t}}{\operatorname{argmin}} \text{NOCT}(x_o, o, v)$   $\triangleright$  Approx.
5:   if  $\hat{u}(x_o, o) = \emptyset$  then
6:      $t_{\text{next}} \leftarrow L$ ; terminate  $\leftarrow$  true
7:   else
8:      $t_{\text{next}} \leftarrow \min\{t' \mid (m, t') \in \hat{u}(x_o, o)\}$ 
9:      $o \leftarrow o \cup \{(m, t_{\text{next}}) \mid (m, t_{\text{next}}) \in \hat{u}(x_o, o)\}$ 
10:   end if
11:   for  $t' = t+1, \dots, t_{\text{next}}$  do
12:     append  $\hat{y}_{t'}(x_{o_{1:t'}})$  to predictions
13:   end for
14:    $t \leftarrow t_{\text{next}}$ 
15: end while
16: return predictions

```

Note that NOCT (Eq. (1)) is not directly tractable at inference time, since it requires knowledge of the ground-truth conditionals $y_{t+1:L}, x_v \mid x_o$; thus, we proceed with estimate of NOCT and $u(x_o, o)$, which we develop below.

3.4. NOCT-Contrastive

In this subsection, we introduce NOCT-Contrastive, an embedding-based estimator that enables estimating $\text{NOCT}(x_o, o, v)$ (and therefore $u(x_o, o)$) from partial observations. We train the embedding space with a contrastive loss that embeds instances according to the utility of future acquisitions.

Plug-in NOCT For *training instances*, $(x_i, y_i) \in \mathcal{D}$, the simplest estimate of $\text{NOCT}(x_{i,o}, o, v)$ (Eq. (1)) is a plug-in sample approach:

$$\widehat{\text{NOCT}}_{pl}(x_{i,o}, o, v) = \ell(x_{i,o} \cup x_{i,v}, y_i, t) + \alpha \sum_{(m, t') \in v} c^m. \quad (3)$$

Note that for a held-out instance, Eq. (3) is not directly computable (it requires future features $x_{i,v}$); we develop inference-time estimators later in this section. For a training instance, we may determine what features are useful when starting from o at time t by ranking candidate future plans $v \subseteq V_{>t}$ using the plug-in objective $\widehat{\text{NOCT}}_{pl}(x_{i,o}, o, v)$ and taking the top- r plans $\hat{v}_{i,o}^{(1)}, \dots, \hat{v}_{i,o}^{(r)}$ with the smallest values. These top plans induce a future-candidate distribution, $\zeta_{i,o}$, over future acquisitions $(m, t') \in V_{>t}$ (and termination \emptyset), where $\zeta_{i,o}(m, t')$ is given by a normalized count of how often (m, t') appears in $\hat{v}_{i,o}^{(1)}, \dots, \hat{v}_{i,o}^{(r)}$. Intuitively, $\zeta_{i,o}$ summarizes which *future* measurements are consistently suggested by the best plans, and we use it in our contrastive loss. The formal $\zeta_{i,o}$ construction in Appx. A.6.

Contrastive Learning We propose to learn an embedding network that maps partially observed features into an embedding space where distances capture the similarity of their acquisition characteristics. Formally, we learn an embedding network $g_\phi(x_{i,o}) \in \mathbb{R}^E$ such that two instances $x_{i,o}$ and $x_{j,o}$ are mapped to nearby points in \mathbb{R}^E if the additional (future) acquisitions available to them are expected to influence their accuracy-cost tradeoff in a similar manner. Conversely, instances with divergent accuracy-cost tradeoff are pushed away in \mathbb{R}^E .

To achieve this, we define a similarity score between instances based on their future-candidate distributions $\zeta_{i,o}$ and $\zeta_{j,o}$, using the exponential of their negative Jensen-Shannon (JS) divergence:

$$\text{sim}_{ij} = \exp(-\beta \text{JS}(\zeta_{i,o}, \zeta_{j,o})), \quad (4)$$

where $\beta > 0$ controls how strongly divergence affects similarity. Letting $\delta_{ij} = \|g_\phi(x_{i,o}) - g_\phi(x_{j,o})\|^2$ be the embedding distance, we minimize a contrastive loss (Chopra et al., 2005):

$$\mathcal{L}_{\text{emb}} = \frac{1}{2} \left(\text{sim}_{ij} \cdot \delta_{ij} + (1 - \text{sim}_{ij}) \cdot \max(0, \gamma - \delta_{ij})^2 \right), \quad (5)$$

where $\gamma > 0$ is the margin parameter. Minimizing \mathcal{L}_{emb} encourages g_ϕ to create an embedding space where distance reflects the similarity of future-candidate distributions.

NOCT-Contrastive For held-out instances (at inference time), the plug-in estimate $\widehat{\text{NOCT}}_{pl}$ in Eq. (3) is unavailable because future measurements and labels are unknown. Instead, we approximate $\text{NOCT}(x_o, o, v)$ by aggregating plug-in values from a small retrieved set of training trajectories selected by the learned embedding:

$$\widehat{\text{NOCT}}(x_o, o, v) \approx \frac{1}{|\mathcal{I}(x_o)|} \sum_{i \in \mathcal{I}(x_o)} \widehat{\text{NOCT}}_{pl}(x_{i,o}, o, v), \quad (6)$$

where $\mathcal{I}(x_o)$ contains the closest training instances induced by g_ϕ : $d(x_o, x_{i,o}) = \|g_\phi(x_o) - g_\phi(x_{i,o})\|_2$ (e.g., by distance thresholding or by selecting the top- K most similar instances). Note that since $g_\phi(x_o)$ embeds instances according to the utility of future acquisition, estimating $\text{NOCT}(x_o, o, v)$ in terms of $\widehat{\text{NOCT}}_{pl}(x_{i,o}, o, v)$ for $i \in \mathcal{I}(x_o)$ is a sound, intuitive strategy. Note further that the size of the embedding space is a controllable hyperparameter, enabling efficiency at small dimensionalities. We call this estimator NOCT-Contrastive.

$\widehat{\text{NOCT}}(x_o, o, v)$ enables us to estimate $\hat{u}(x_o, o)$ in Alg. 1, to plan acquisitions at inference time. In practice, instead of an exhaustive search over $v \subseteq V_{>t}$, one may consider a distributionally sampled (e.g., uniform random or feature-importance guided) set of candidate plans. More sophisticated discrete optimizers could be substituted if desired, but typically introduce additional overhead (Parker and Rardin, 2014; Rajeev and Krishnamoorthy, 1992).

3.5. NOCT-Amortized

We now develop NOCT-Amortized, a complementary approach that amortizes inference and predicts the NOCT value for candidate acquisition plans using a neural network.

Neural NOCT estimator We learn an estimator f_θ that predicts the NOCT value of a candidate plan from the *partial information* x_o . Since future features x_v are unknown at inference time, f_θ is conditioned on the partial observations x_o , a representation of the candidate plan v (e.g., a binary mask over feature-time pairs in $V_{>t}$), and the current time t :

$$f_\theta(x_o, v, t) \approx \text{NOCT}(x_o, o, v). \quad (7)$$

At inference time, we substitute Eq. (7) into Alg. 1 and obtain the future candidate plan:

$$\hat{u}(x_o, o) \in \arg \min_{v \subseteq V_{>t}} f_\theta(x_o, v, t). \quad (8)$$

Training Objective During training, we can compute the plug-in target $\widehat{\text{NOCT}}_{pl}(x_o, o, v)$ in Eq. (3) because the ground-truth future values for x_v are available in \mathcal{D} . We train f_θ by minimizing the mean squared error objective:

$$\mathcal{L}_{\text{amort}} = (f_\theta(x_o, v, t) - \widehat{\text{NOCT}}_{pl}(x_o, o, v))^2. \quad (9)$$

Joint Fine-tuning with the Predictor To reduce the mismatch between (i) the partially observed inputs used by the predictor \hat{y} and (ii) the inputs scored by f_θ during planning, we jointly fine-tune f_θ and \hat{y} with

$$\mathcal{L}_{\text{joint}} = \frac{1}{L} \sum_{k=1}^L \text{CE}(\hat{y}_k(x_{o_{1:k}}), y_k) + \lambda \mathcal{L}_{\text{amort}}, \quad (10)$$

where λ trades off predictive accuracy and utility estimation.

4. Experiments

4.1. Datasets

Synthetic Inspired by [Kossen et al. \(2023\)](#), we construct a synthetic dataset of $N = 8,000$ samples with $L = 10$ non-i.i.d. timepoints. Each timepoint contains two features: *digit* and *counter*. Labels are the cumulative sum of the digits, when the counter values are zero. We elaborate below.

The *digit* feature is a sequence of uniformly random L integers from $\{0, 1, 2\}$, e.g., 1010220110. The *counter* feature is created by concatenating countdown sequences that begin with randomly chosen starting values from $\{0, 1, 2\}$ and truncating to a fixed length of L . For example, starting values 2, 1, 2, and 1 yield 210, 10, 210, 10, and the final counter feature is their concatenation 2101021010 (of length L). Unlike [Kossen et al. \(2023\)](#), we assign labels at every timestep: $y_t = \sum_{t'=1}^t \text{digit}_{t'} \mathbb{I}\{\text{counter}_{t'} = 0\}$; for example, label 0011333444 in the case of $\text{counter: } 2101021010$ and $\text{digit: } 1010220110$. The policy should begin with acquiring the digit and counter at $t = 1$, then acquiring the digit at the next anticipated timestep where $\text{counter} = 0$, then acquiring the *counter* again to locate the next $\text{counter} = 0$ timestep, and repeat. Following [Kossen et al. \(2023\)](#), we split data into train/val/test (70%/15%/15%).

ADNI The Alzheimer’s Disease Neuroimaging Initiative (ADNI) dataset³ ([Petersen et al., 2010](#)) is a longitudinal, multi-center, observational study. Patients are categorized into cognitively unimpaired, mild cognitive impairment, and Alzheimer’s Disease ([O’Bryant et al., 2008; 2010](#)). Following [Qin et al. \(2024\)](#), we use $N = 1,002$ patients with four biomarkers extracted from PET (FDG and AV45) and MRI (Hippocampus and Entorhinal) across $L = 12$ visits, and split the dataset into train/val/test (64%/16%/20%).

OAI The Osteoarthritis Initiative (OAI) dataset⁴ contains $N = 4,796$ patients (left/right knees) monitored up to 96 months. We use the tabular data from [Chen et al. \(2024\)](#) and joint space width, totaling 27 features per visit across $L = 7$ visits. We predict the two clinical scores: Kellgren-Lawrence grade (KLG) ([Kellgren et al., 1957](#)) (range $0 \sim 4$) and WOMAC pain score ([McConnell et al., 2001](#)) (range

$0 \sim 20$). Following previous works ([Chen et al., 2024](#); [Nguyen et al., 2024](#)), we merge KLG = 0 and 1, and define WOMAC < 5 as no pain and ≥ 5 as pain, and split the dataset into train/val/test (50%/12.5%/37.5%).

4.2. Baselines

We expand the comparisons performed in recent work by [Qin et al. \(2024\)](#) in longitudinal AFA by comparing to two other state-of-the-art AFA methods, DIME ([Gadgil et al., 2024](#)) and DiFA ([Ghosh and Lan, 2023](#)), in addition to the RL method considered by [Qin et al. \(2024\)](#).

In total, we consider the following baselines: 1) **ASAC** ([Yoon et al., 2019](#)): an actor-critic method to jointly train a feature selector and a predictor network; 2) **RAS** ([Qin et al., 2024](#)): an RL approach to decide when and which features to capture for longitudinal data where the predicted acquisition times are continuous and not restricted to certain discrete timepoints; 3) **AS** ([Qin et al., 2024](#)): RAS with a constant acquisition interval; 4) **DIME** ([Gadgil et al., 2024](#)): a greedy method to sequentially select the most informative features; 5) **DiFA** ([Ghosh and Lan, 2023](#)): a Gumbel-softmax-based differentiable policy. For each baseline, we perform a comparable hyperparameter search on the validation set using the authors’ original code, and report test performance under the selected configuration. We also verify reproduction of reported results (e.g., RAS on ADNI); full details are provided in Appx. B.2.

We adapt DIME and DiFA for longitudinal data by restricting acquisitions to either the current or future time points. Note that DIME and DiFA acquire features one at a time, allowing repeated selection within the same time step t , while NOCTA and other baselines simultaneously select all desired features at t before moving to the next time steps. An advantage of DiFA and DIME is that they can acquire more tests now or move to the next visit.

4.3. Implementation

Data Availability and Missingness. Unlike standard AFA methods that assume fully observed data ([Rahbar et al., 2025](#); [Shim et al., 2018](#); [Nan et al., 2015](#)), our work is general and handles missingness completely at random. This is done by excluding missing features from candidate sets and pretraining the prediction network \hat{y}_k , estimator f_θ , and embedding network g_ϕ with random input-feature dropout.

Prediction Network Implementation. At each time t , the prediction network predicts outcomes at future timepoints \hat{y}_k , $k \geq t$. We train an MLP that takes all the features observed up to time t , denoted $x_{o_{1:t}}$ ⁵ and the future time

³<https://adni.loni.usc.edu>
⁴<https://nda.nih.gov/oai/>

⁵ x_o may contain missingness inherent to the data collection process. Additionally, unobserved features (missing or not acquired) are being masked out during implementation.

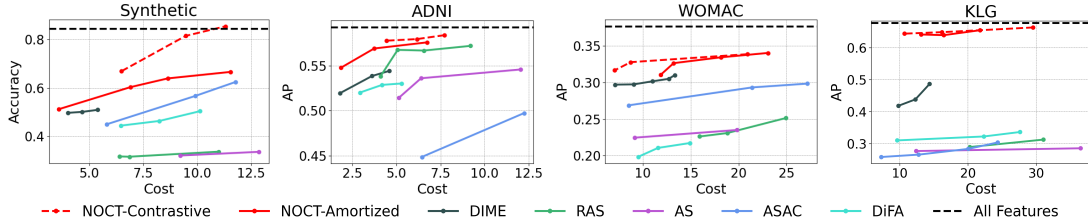


Figure 3. Performance/cost of models across various average acquisition costs (budgets). Following (Kossen et al., 2023), we show accuracy rather than average precision for the synthetic dataset. Our NOCT estimators show the highest accuracy for a given cost.

indicator k . For predictions at $k > t$, the network must predict without access to any additional features beyond those observed by time t (i.e., $\hat{y}_k(x_{o_{1:t}})$ for $k > t$).

NOCT-Contrastive Implementation. We train the MLP predictor \hat{y}_k and then train the MLP embedding network g_ϕ . We set $\beta = \gamma = 1$, $K = 5$, and embedding dimension $E = 32$ (Synthetic/ADNI) and $E = 64$ (OAI).

NOCT-Amortized Implementation. We first train the MLP predictor \hat{y}_k , followed by jointly fine-tuning the predictor and the MLP-based NOCT estimator f_θ (Eq. 9) using $\lambda = 1$.

Optimizer and Inference We utilize Adam (Kingma and Ba, 2015) with a learning rate of 10^{-3} . At each inference step, we evaluate a subset of 1,000 plans from the candidate space (see Appx. A.7 for a stability analysis).

We report predictive performance results as the mean over five independent runs (standard errors for each run are provided in Appx. C). Feature costs and further details on the experimental setup can be found in Appx. B. Moreover, Appx. A.7 shows a hyperparameter sensitivity analysis, demonstrating that *our method remains robust across different settings and can be applied without extensive tuning*. Upon publication, we will make our code publicly available.

4.4. Performance-Cost Results

Fig. 3 shows results across different datasets. For each figure, the x-axis represents different average acquisition costs per instance, and the y-axis represents the performance. As the budget increases, more features can be acquired, and prediction performance typically improves. We varied hyperparameters to obtain prediction results under different average acquisition costs. Details on the performance-cost tradeoff hyperparameters for each method are in Appx. B.

Synthetic Dataset. Following Kossen et al. (2023), we use accuracy for performance on the synthetic dataset. The NOCT-Contrastive estimator outperforms the baselines, followed by the NOCT-Amortized estimator, suggesting that the baseline methods may not adequately model dependencies between features and necessary acquisitions.

ADNI Dataset. Following Qin et al. (2024), we show the average precision (AP) result for different costs. Both estimator variants of NOCTA consistently outperform all other baseline methods while using lower overall acquisition cost.

OAI Dataset. We report AP on KLG and WOMAC prediction (Fig. 3). The NOCTA again outperforms the baselines, while RL-based approaches (ASAC, AS, and RAS) underperform compared to the greedy approach (DIME), suggesting that RL-based frameworks may struggle with the complexity and noise of longitudinal feature acquisition.

Overall, our NOCT-Contrastive estimator achieves the highest accuracy across benchmarks, and our NOCT-Amortized estimator achieves comparable performance while avoiding retrieval-based search at inference time. AUC ROC results (Appx. C) show a similar trend; time complexity analysis is in Appx. A.3.

4.5. Ablation of NOCT-Contrastive Embedding

We evaluate the effectiveness of the learned representation in the similarity-based retrieval step by forming the retrieved reference set $\mathcal{I}(\cdot)$ using the learned representation g_ϕ versus (i) using the native feature values and (ii) using the last hidden layer from the predictor \hat{y} . For any two samples x_i and x_j having the same observed feature set o , we define *Euclidean distance on observed features* as $d(x_{i,o}, x_{j,o}) = \|x_{i,o} - x_{j,o}\|_2$. Moreover, using *the predictor embedding* $h(\cdot)$ (the last hidden layer of \hat{y}_k), we compute the corresponding distance as $d(x_{i,o}, x_{j,o}) = \|h(x_{i,o}) - h(x_{j,o})\|_2$. Tab. 1 shows results under two cost regimes (low and high): our contrastive approach is robust to the retrieval metric, and $g_\phi(\cdot)$ outperforms both the native feature values and $h(\cdot)$ on ADNI and WOMAC, with comparable results on KLG. Notably, on ADNI, the low-cost result for $g_\phi(\cdot)$ (cost = 4.343) already outperforms the high-cost performance of both alternatives (cost = 7.866 and 10.297). This indicates that *the embedding network is able to learn informative representations for real-world longitudinal AFA tasks*.

4.6. Acquisition Trajectory Analysis

Fig. 4 highlights why NOCTA’s acquisition behavior differs from RL- and greedy-based baselines. NOCTA typi-

Table 1. Result comparisons of using the feature values, \hat{y} prediction embedding (last hidden layer), and learned representation $g_\phi(\cdot)$ to gather instances for NOCT-Contrastive inference. We report the mean \pm standard errors across five runs.

METHOD	ADNI			WOMAC			KLG		
	AP	ROC	COST	AP	ROC	COST	AP	ROC	COST
FEATURE VALUES	0.545 \pm 0.004	0.727 \pm 0.002	7.052 \pm 0.069	0.315 \pm 0.003	0.617 \pm 0.004	9.014 \pm 2.863	0.629 \pm 0.003	0.821 \pm 0.002	11.024 \pm 0.011
PREDICTION EMBEDDING	0.567 \pm 0.005	0.744 \pm 0.004	6.218 \pm 0.038	0.290 \pm 0.005	0.618 \pm 0.002	6.998 \pm 0.023	0.639 \pm 0.004	0.825 \pm 0.002	13.706 \pm 0.055
EMBEDDING NETWORK	0.578 \pm 0.004	0.760 \pm 0.003	4.434 \pm 0.042	0.328 \pm 0.004	0.646 \pm 0.003	8.729 \pm 0.011	0.644 \pm 0.003	0.822 \pm 0.001	10.687 \pm 0.018
	0.584 \pm 0.013	0.760 \pm 0.006	7.727 \pm 0.094	0.339 \pm 0.008	0.647 \pm 0.003	20.921 \pm 0.058	0.649 \pm 0.002	0.822 \pm 0.002	16.192 \pm 0.062

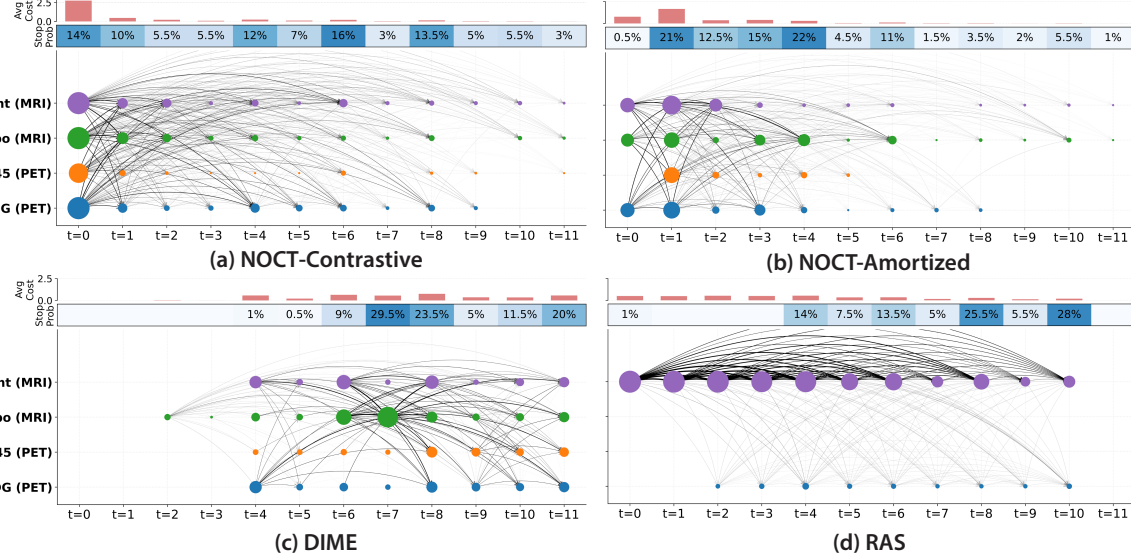


Figure 4. Qualitative comparison of acquisition dynamics on the test set of the ADNI dataset (regular follow-ups every six months). For each method, **top** shows the average acquisition cost at each timepoint (mean per sample), and **middle** shows the termination distribution that occurred at each timepoint. The **bottom** panel visualizes feature-time acquisition as a directed graph: each node corresponds to a feature acquired at a specific timepoint, and node size shows how often that feature is acquired at that time. A directed arrow from (m, t) to (m', t') (with $t' > t$) indicates the frequent co-acquisition across time, i.e., samples that acquire (m, t) also acquire (m', t') later. Average acquisition cost per sample: 4.3775 (NOCT-Contrastive), 3.7425 (NOCT-Amortized), 4.0475 (DIME), and 3.9750 (RAS).

cally acquires early because, in longitudinal settings, early measurements reduce uncertainty for later timepoints and cannot be reacquired once missed; this holds for both NOCT-Contrastive and NOCT-Amortized estimators. Moreover, NOCTA terminates at varying timepoints once the expected benefit of additional measurements no longer justifies their cost. In contrast, RL-trained RAS converges to a local maximum of repeatedly selecting the same measurements as a reliable uncertainty-reduction strategy. Meanwhile, the greedy-based approach DIME does not account for a time-based strategy, and instead directly jumps into the future to acquire at the marginally most informative timepoint. In a longitudinal setting, this can undervalue early measurements whose benefits are realized only when combining with later measurements, and it can prevent acquisitions in early time points after committing to a greedy future acquisition. Overall, NOCTA yields earlier, more selective acquisitions with adaptive stopping, whereas RAS repeatedly reacquires and DIME delays its measurements.

5. Conclusion

In this work, we proposed NOCTA, a non-greedy longitudinal active feature acquisition framework that directly trades off acquisition cost and predictive performance under temporal dynamics. Central to NOCTA is the NOCT objective, which provides a unified target for evaluating future acquisition plans from partial observations, together with two complementary estimators: NOCT-Contrastive and NOCT-Amortized. Experiments on synthetic benchmarks and real-world medical datasets demonstrate that NOCTA consistently outperforms baseline methods while achieving lower overall acquisition cost. While the NOCT-Contrastive estimator offers strong and robust performance, the NOCT-Amortized estimator attains comparable results with fast amortized inference. In practice, both variants support model selection via validation (or ensembling) to obtain a single deployed policy.

Acknowledgements

This research was, in part, funded by the National Institutes of Health (NIH) under awards 1OT2OD038045-01, NIAMS 1R01AR082684, 1R01AA02687901A1, and 1OT2OD032581-02-321, and was partially funded by the National Science Foundation (NSF) under grants IIS2133595 and DMS2324394. The views and conclusions contained in this document are those of the authors and should not be interpreted as representing official policies, either expressed or implied, of the NIH and NSF.

Impact Statement

In this paper, we introduce a non-greedy active feature acquisition framework, NOCTA, which could aid the decision-making process in real-world applications such as healthcare. Specifically, NOCTA could provide a more efficient and cost-effective diagnosis by selectively acquiring essential medical examinations, thus minimizing patient burden (e.g., time and costs) through personalized and timely intervention. However, as in any ML system, using NOCTA should involve thorough/robust evaluations and supervision by medical professionals to prevent any potential negative impact.

References

Boqi Chen, Junier Oliva, and Marc Niethammer. A unified model for longitudinal multi-modal multi-view prediction with missingness. In *International Conference on Medical Image Computing and Computer-Assisted Intervention*, pages 410–420. Springer, 2024.

Sumit Chopra, Raia Hadsell, and Yann LeCun. Learning a similarity metric discriminatively, with application to face verification. In *2005 IEEE computer society conference on computer vision and pattern recognition (CVPR’05)*, volume 1, pages 539–546. IEEE, 2005.

Ian Connick Covert, Wei Qiu, Mingyu Lu, Na Yoon Kim, Nathan J White, and Su-In Lee. Learning to maximize mutual information for dynamic feature selection. In *International Conference on Machine Learning*, pages 6424–6447. PMLR, 2023.

Adam Dunkels, Joakim Eriksson, Niclas Finne, and Nicolas Tsiftes. Powertrace: Network-level power profiling for low-power wireless networks, 2011.

Soham Gadgil, Ian Connick Covert, and Su-In Lee. Estimating conditional mutual information for dynamic feature selection. In *The Twelfth International Conference on Learning Representations*, 2024.

Aritra Ghosh and Andrew Lan. Difa: Differentiable feature acquisition. In *Proceedings of the AAAI Conference on Artificial Intelligence*, volume 37, pages 7705–7713, 2023.

Wenbo Gong, Sebastian Tschiatschek, Sebastian Nowozin, Richard E Turner, José Miguel Hernández-Lobato, and Cheng Zhang. Icebreaker: Element-wise efficient information acquisition with a bayesian deep latent gaussian model. *Advances in neural information processing systems*, 32, 2019.

Oleg Ivanov, Michael Figurnov, and Dmitry Vetrov. Variational autoencoder with arbitrary conditioning. In *International Conference on Learning Representations*, 2019. URL <https://openreview.net/forum?id=SyxtJh0qYm>.

Jaromír Janisch, Tomáš Pevný, and Viliam Lisý. Classification with costly features as a sequential decision-making problem. *Machine Learning*, 109(8):1587–1615, 2020.

Jonas H Kellgren, JS Lawrence, et al. Radiological assessment of osteo-arthrosis. *Ann Rheum Dis*, 16(4):494–502, 1957.

Patrick Kidger, James Morrill, James Foster, and Terry Lyons. Neural controlled differential equations for irregular time series. *Advances in Neural Information Processing Systems*, 33:6696–6707, 2020.

Diederik P. Kingma and Jimmy Ba. Adam: A method for stochastic optimization. In *International Conference on Learning Representations (ICLR)*, 2015.

Jannik Kossen, Cătălina Cangea, Eszter Vértes, Andrew Jaegle, Viorica Patraucean, Ira Ktena, Nenad Tomasev, and Danielle Belgrave. Active acquisition for multimodal temporal data: A challenging decision-making task. *Transactions on Machine Learning Research*, 2023.

Yang Li and Junier Oliva. Active feature acquisition with generative surrogate models. In *International conference on machine learning*, pages 6450–6459. PMLR, 2021.

Chao Ma, Sebastian Tschiatschek, Konstantina Palla, Jose Miguel Hernandez-Lobato, Sebastian Nowozin, and Cheng Zhang. Eddi: Efficient dynamic discovery of high-value information with partial vae. In *International Conference on Machine Learning*, pages 4234–4243. PMLR, 2019.

Sara McConnell, Pamela Kolopack, and Aileen M Davis. The western ontario and mcmaster universities osteoarthritis index (womac): a review of its utility and measurement properties. *Arthritis Care & Research: Official Journal of the American College of Rheumatology*, 45(5):453–461, 2001.

Mahathir Monjur, Yubo Luo, Zhenyu Wang, and Shahriar Nirjon. Soundsieve: Seconds-long audio event recognition on intermittently-powered systems. In *Proceedings of the 21st Annual International Conference on Mobile Systems, Applications and Services*, pages 28–41, 2023.

Feng Nan, Joseph Wang, and Venkatesh Saligrama. Feature-budgeted random forest. In *International conference on machine learning*, pages 1983–1991. PMLR, 2015.

Khanh Nguyen, Huy Hoang Nguyen, Egor Panfilov, and Aleksei Tiulpin. Active sensing of knee osteoarthritis progression with reinforcement learning. *arXiv preprint arXiv:2408.02349*, 2024.

Sid E O’Bryant, Stephen C Waring, C Munro Cullum, James Hall, Laura Lacritz, Paul J Massman, Philip J Lupo, Joan S Reisch, Rachelle Doody, Texas Alzheimer’s Research Consortium, et al. Staging dementia using clinical dementia rating scale sum of boxes scores: a texas alzheimer’s research consortium study. *Archives of neurology*, 65(8):1091–1095, 2008.

Sid E O’Bryant, Laura H Lacritz, James Hall, Stephen C Waring, Wenyaw Chan, Zeina G Khodr, Paul J Massman, Valerie Hobson, and C Munro Cullum. Validation of the new interpretive guidelines for the clinical dementia rating scale sum of boxes score in the national alzheimer’s coordinating center database. *Archives of neurology*, 67(6):746–749, 2010.

R Gary Parker and Ronald L Rardin. *Discrete optimization*. Elsevier, 2014.

Ronald Carl Petersen, Paul S Aisen, Laurel A Beckett, Michael C Donohue, Anthony Collins Gamst, Danielle J Harvey, CR Jack Jr, William J Jagust, Leslie M Shaw, Arthur W Toga, et al. Alzheimer’s disease neuroimaging initiative (adni) clinical characterization. *Neurology*, 74(3):201–209, 2010.

Yuchao Qin, Mihaela van der Schaar, and Changhee Lee. Risk-averse active sensing for timely outcome prediction under cost pressure. *Advances in Neural Information Processing Systems*, 36, 2024.

Arman Rahbar, Linus Aronsson, and Morteza Haghir Chehreghani. A survey on active feature acquisition strategies. *arXiv preprint arXiv:2502.11067*, 2025.

Srijith Rajeev and CS Krishnamoorthy. Discrete optimization of structures using genetic algorithms. *Journal of structural engineering*, 118(5):1233–1250, 1992.

Maytal Saar-Tsechansky, Prem Melville, and Foster Provost. Active feature-value acquisition. *Management Science*, 55(4):664–684, 2009.

Victor S Sheng and Charles X Ling. Feature value acquisition in testing: a sequential batch test algorithm. In *Proceedings of the 23rd international conference on Machine learning*, pages 809–816, 2006.

Hajin Shim, Sung Ju Hwang, and Eunho Yang. Joint active feature acquisition and classification with variable-size set encoding. *Advances in neural information processing systems*, 31, 2018.

Michael Valancius, Maxwell Lennon, and Junier Oliva. Acquisition conditioned oracle for nongreedy active feature acquisition. In *International Conference on Machine Learning*, pages 48957–48975. PMLR, 2024.

Haiyan Yin, Yingzhen Li, Sinno Jialin Pan, Cheng Zhang, and Sebastian Tschiatschek. Reinforcement learning with efficient active feature acquisition. *arXiv preprint arXiv:2011.00825*, 2020.

Jinsung Yoon, James Jordon, and Mihaela Schaar. Asac: Active sensing using actor-critic models. In *Machine Learning for Healthcare Conference*, pages 451–473. PMLR, 2019.

Daphney-Stavroula Zois and Urbashi Mitra. Active state tracking with sensing costs: Analysis of two-states and methods for n -states. *IEEE Transactions on Signal Processing*, 65(11):2828–2843, 2017.

Appendix

A. Additional Discussion

A.1. Broader Application

We acknowledge that our experiments focus on the healthcare domain, an important application area; however, our method is not specific to any domain. Similar resource-constrained scenarios also exist in other domains, such as in energy-aware audio recognition (Monjur et al., 2023) or IoT devices (Dunkels et al., 2011). In fact, our AFA formulation has applications across a myriad of domains, including robotics (acquisition of sensors with resource constraints), education (acquisition of different exam types without overburdening students), and beyond.

A.2. Assumptions & Limitations

Like traditional AFA methods and RL-based baselines, NOCTA assumes that the problem has a finite horizon with a limited number of time steps. Additionally, we acknowledge that, similar to other baselines presented in this paper, the performance of NOCTA is sensitive to the data quality. In particular, poor label annotation in real-world clinical datasets can degrade the accuracy. However, extending to an infinite-horizon setting and mitigating the sensitivity to the data quality are beyond the scope of this paper. We will leave these challenges for future work.

A.3. Time Complexity

With a total of time steps L and a total number of features M , the time complexity is $O(ML^2)$ for RL baselines (RAS, AS, ASAC), and $O(M^2L^2)$ for DiFA and DIME. For neural estimator NOCT-Amortized, with a random subset search of size $|\mathcal{O}|$ (i.e., number of candidate plans), the time complexity is $O(ML^2|\mathcal{O}|)$. However, if one wants to incorporate the instance-based estimator NOCT-Contrastive with the number of training points n , the time complexity is $O(nML^2|\mathcal{O}|)$, where a naive similarity-based retrieval over the n training embeddings costs $O(nML)$. Note that both estimators can further parallelize the $|\mathcal{O}|$ subsets across independent workers.

A.4. Proof of Theorem 3.1: –NOCT Lower Bounds the Optimal Longitudinal AFA MDP Value

Theorem 3.1. (Informal) –NOCT lower bounds the value of the optimal longitudinal AFA MDP policy

Problem Setup. For any observations (x_o, o, t) , let the set of remaining feature-time pairs that are still available after time t be:

$$\mathcal{V}_{>t} = \{(m, t') \mid m \in \{1, \dots, M\}, t' \in \{t+1, \dots, L\}\}.$$

To follow the convention of reinforcement learning literature, we redefine the objective NOCT (Eq. (1)) as maximization instead of minimization without loss of generality. For notational convenience, we write $\text{NOCT-MAX}_t^s(x_o) \equiv \text{NOCT-MAX}_t^s(x_o, o)$, since x_o is indexed by the observation set o . That is, for any partial observation (x_o, o, t) , we define $\text{NOCT-MAX}_t^s(x_o)$ as:

$$\text{NOCT-MAX}_t^s(x_o) := \max_{\substack{v \subseteq \mathcal{V}_{>t} \\ \text{s.t. } |\text{rounds}(v)| \leq s}} \left[-\mathbb{E}_{y_{t+1:L}, x_v | x_o} [\ell(x_o \cup x_v, y, t)] - \alpha \sum_{(m, t') \in v} c^m \right],$$

where $s \in \mathbb{N}$ represents the maximum number of possible future acquisition rounds, and let $\text{rounds}(v) := \{t' \mid \exists m \in \{1, \dots, M\} : (m, t') \in v\}$. We then define

$$V_t^0(x_o) := -\mathbb{E}_{y_{t+1:L} | x_o} [\ell(x_o, y, t)]$$

and

$$V_t^s(x_o) := \max \left\{ V_t^0(x_o), \max_{\substack{t' \in \{t+1, \dots, L\} \\ a_{t'} \in \{0, 1\}^M}} \left[-\alpha \sum_m a_{t', m} c^m + \mathbb{E}_{x_{a_{t'}} | x_o} [V_{t'}^{s-1}(x_o \cup a_{t'})] \right] \right\}. \quad (11)$$

We see that V_t^0 is the expected negative cumulative loss when we immediately terminate at t , and we predict the future labels using only what we have acquired so far, x_o . Thus, V_t^s is the value for the optimal longitudinal AFA policy, such

that it either (i) terminates, returning V_t^0 or (ii) executes another acquisition at the future time step $t' \in (t+1, \dots, L)$ and acquires the feature $a_{t'} \in \{0, 1\}^M$.

Claim. For every (x_o, o, t) with $s \in \mathbb{N}_{\geq 0}$, we have $V_t^s(x_o) \geq \text{NOCT-MAX}_t^s(x_o)$.

Proof.

Base case $s = 0$. Since there is no further action, both the MDP agent and NOCT-MAX terminate:

$$V_t^0(x_o) = -\mathbb{E}_{y_{t+1:L}|x_o}[\ell(x_o, y, t)] = \text{NOCT-MAX}_t^0(x_o).$$

Inductive hypothesis. Assume for $s-1 \geq 0$, we have:

$$V_{t'}^{s-1}(x) \geq \text{NOCT-MAX}_{t'}^{s-1}(x) \quad \forall (x, t'). \quad (\text{IH})$$

Inductive step. We fix (x_o, t) and see that:

$$\begin{aligned} & V_t^s(x_o) \\ &= \max \left\{ V_t^0(x_o), \max_{\substack{t' \in \{t+1, \dots, L\} \\ a_{t'} \in \{0, 1\}^M}} \left[-\alpha \sum_m a_{t',m} c^m + \mathbb{E}_{x_{a_{t'}}|x_o} [V_{t'}^{s-1}(x_o \cup a_{t'})] \right] \right\} \\ &\stackrel{(\text{IH})}{\geq} \max \left\{ V_t^0(x_o), \max_{\substack{t' \in \{t+1, \dots, L\} \\ a_{t'} \in \{0, 1\}^M}} \left[-\alpha \sum_m a_{t',m} c^m + \mathbb{E}_{x_{a_{t'}}|x_o} [\text{NOCT-MAX}_{t'}^{s-1}(x_o \cup a_{t'})] \right] \right\} \\ &= \max \left\{ V_t^0(x_o), \right. \\ &\quad \left. \max_{\substack{t' \in \{t+1, \dots, L\} \\ a_{t'} \in \{0, 1\}^M}} \left[-\alpha \sum_m a_{t',m} c^m + \mathbb{E}_{x_{a_{t'}}|x_o} \left[\max_{\substack{v' \subseteq \mathcal{V}_{>t'} \\ \text{s.t. } |\text{rounds}(v')| \leq s-1}} \left(-\mathbb{E}_{y_{t'+1:L}, x_{v'}|x_o, x_{a_{t'}}} [\ell(x_o \cup x_{a_{t'}} \cup x_{v'}, y, t')] - \alpha \sum_{(m, t'') \in v'} c^m \right) \right] \right] \right\} \\ &\stackrel{*}{\geq} \max \left\{ V_t^0(x_o), \right. \\ &\quad \left. \max_{\substack{t' \in \{t+1, \dots, L\} \\ a_{t'} \in \{0, 1\}^M}} \max_{\substack{v' \subseteq \mathcal{V}_{>t'} \\ \text{s.t. } |\text{rounds}(v')| \leq s-1}} \left[-\mathbb{E}_{y_{t'+1:L}, x_{v'}, x_{a_{t'}}|x_o} [\ell(x_o \cup x_{a_{t'}} \cup x_{v'}, y, t')] - \alpha \left(\sum_{(m, t'') \in v'} c^m + \sum_m a_{t',m} c^m \right) \right] \right\} \\ &= \max \left\{ V_t^0(x_o), \max_{\substack{v \in \mathcal{V}_{>t} \\ \text{s.t. } |\text{rounds}(v)| \leq s}} \left[-\mathbb{E}_{y_{t+1:L}, x_v|x_o} [\ell(x_o \cup x_v, y, t)] - \alpha \sum_{(m, t'') \in v} c^m \right] \right\} \\ &= \text{NOCT-MAX}_t^s(x_o). \end{aligned}$$

where * follows from:

$$\begin{aligned} \forall v' \in \Omega, x_{a_{t'}}, \max_{v \in \Omega} \mathcal{L}(x_{a_{t'}}, v) &\geq \mathcal{L}(x_{a_{t'}}, v') \implies \\ \forall v' \in \Omega, \mathbb{E}_{x_{a_{t'}}|x_o} \left[\max_{v \in \Omega} \mathcal{L}(x_{a_{t'}}, v) \right] &\geq \mathbb{E}_{x_{a_{t'}}|x_o} [\mathcal{L}(x_{a_{t'}}, v')] \implies \\ \mathbb{E}_{x_{a_{t'}}|x_o} \left[\max_{v \in \Omega} \mathcal{L}(x_{a_{t'}}, v) \right] &\geq \max_{v \in \Omega} \mathbb{E}_{x_{a_{t'}}|x_o} [\mathcal{L}(x_{a_{t'}}, v)] \end{aligned}$$

for $\Omega := \{v \subseteq \mathcal{V}_{>t'} \mid |\text{rounds}(v)| \leq s-1\}$ and

$$\mathcal{L}(x_{a_{t'}}, v) := -\mathbb{E}_{y_{t+1:L}, x_{v'}|x_o, x_{a_{t'}}} [\ell(x_o \cup x_{a_{t'}} \cup x_{v'}, y, t')] - \alpha \left(\sum_{(m, t'') \in v'} c^m + \sum_m a_{t',m} c^m \right).$$

Note that one may recover the non-cardinality constrained problem by considering large enough s , yielding a lower bound on the longitudinal AFA MDP.

A.5. Proof of Proposition 3.2: Dynamic Replanning is Never Worse

Proposition 3.2. (Informal) *Replanning after each acquisition is never worse (in terms of the NOCT objective) than committing to the original plan's remainder.*

Problem Setup. Fix any observation state (x_o, o, t) and let the set of all feature-time pairs that are available be: $\mathcal{V}_{>t} := \{(m, t') : t < t' \leq L\}$. Let the current plan be

$$u(x_o, o) \in \arg \min_{v \subseteq \mathcal{V}_{>t}} \text{NOCT}(x_o, o, v).$$

If $u(x_o, o) = \emptyset$, then we stop the acquisition and the claim is trivial. Otherwise, we define the next acquisition time t_{next} and the set of acquisitions $a_{t_{\text{next}}}$ at time t_{next} be:

$$t_{\text{next}} := \min\{t' : (m, t') \in u(x_o, o)\}, \quad a_{t_{\text{next}}} := \{(m, t_{\text{next}}) \in u(x_o, o)\}.$$

After observing $x_{a_{t_{\text{next}}}}$, we update the current observed features $o' := o \cup a_{t_{\text{next}}}$ and $x_{o'} := x_o \cup x_{a_{t_{\text{next}}}}$, and define the remainder of the original plan after t_{next} :

$$\tilde{u} := \{(m, \tau) \in u(x_o, o) : \tau > t_{\text{next}}\} \subseteq \mathcal{V}_{>t_{\text{next}}}.$$

NOCT of the original strategy: We can decompose NOCT by splitting the loss sum at t_{next} and splitting the costs into those at t_{next} and those after t_{next} . This yields:

$$\begin{aligned} \text{NOCT}(x_o, o, u(x_o, o)) &= \mathbb{E}_{y_{t+1:t_{\text{next}}}, x_{a_{t_{\text{next}}}} | x_o} \left[\sum_{k=t+1}^{t_{\text{next}}} \text{CE}(\hat{y}_k(x_o \cup x_{u(x_o, o)^{t+1:k}}), y_k) \right] + \alpha \sum_{(m, t_{\text{next}}) \in a_{t_{\text{next}}}} c_m \\ &\quad + \mathbb{E}_{x_{a_{t_{\text{next}}}} | x_o} [\text{NOCT}(x'_o, o', \tilde{u})], \end{aligned} \quad (12)$$

where $u(x_o, o)^{t+1:k}$ denotes the subset of original plan $u(x_o, o)$ restricted to times $t+1, \dots, k$.

NOCT of the replanning strategy: Let $\mathcal{R}(x_o, o, t)$ denote the expected NOCT objective by the replanning strategy that repeats: (i) compute $u(\cdot)$ via Eq. (2), (ii) execute its next acquisition $(t_{\text{next}}, a_{t_{\text{next}}})$, (iii) update (x_o, o, t) , and (iv) repeat step (i) (Alg. 1). With this definition, $\mathcal{R}(x_o, o, t)$ is the recursion defined as:

$$\begin{aligned} \mathcal{R}(x_o, o, t) &= \mathbb{E}_{y_{t+1:t_{\text{next}}}, x_{a_{t_{\text{next}}}} | x_o} \left[\sum_{k=t+1}^{t_{\text{next}}} \text{CE}(\hat{y}_k(x_o \cup x_{u(x_o, o)^{t+1:k}}), y_k) \right] + \alpha \sum_{(m, t_{\text{next}}) \in a_{t_{\text{next}}}} c_m \\ &\quad + \mathbb{E}_{x_{a_{t_{\text{next}}}} | x_o} [\mathcal{R}(x'_o, o', t_{\text{next}})]. \end{aligned} \quad (13)$$

Please note that the first two terms in Eq. (13) match with those in Eq. (12) because both strategies execute the same first acquisition at t_{next} and thus make identical predictions up to t_{next} ; *the only difference is the continuation* (we will utilize this fact later in the proof).

Claim. For all (x_o, o, t) , $\mathcal{R}(x_o, o, t) \leq \text{NOCT}(x_o, o, u(x_o, o))$.

Proof.

We will prove this with backward induction.

Base case. The base case is $t = L$ (i.e., $\mathcal{V}_{>t} = \emptyset$), where both strategies terminate immediately and are equal.

Inductive hypothesis. Assume that for every state $(\bar{x}_o, \bar{o}, \bar{t})$ with smaller remaining horizon (i.e., $L - \bar{t} < L - t$), we have:

$$\mathcal{R}(\bar{x}_o, \bar{o}, \bar{t}) \leq \text{NOCT}(\bar{x}_o, \bar{o}, u(\bar{x}_o, \bar{o})). \quad (14)$$

Inductive step. We fix (x_o, o, t) with $u(x_o, o) \neq \emptyset$ and the corresponding $t_{\text{next}}, a_{t_{\text{next}}}, (x'_o, o')$ defined above. Since $t_{\text{next}} > t$, we have $L - t_{\text{next}} < L - t$, so the induction hypothesis Eq. (14) applies at $(x'_o, o', t_{\text{next}})$:

$$\mathcal{R}(x'_o, o', t_{\text{next}}) \leq \text{NOCT}(x'_o, o', u(x'_o, o')). \quad (15)$$

Moreover, by optimality of $u(x'_o, o')$ at state $(x'_o, o', t_{\text{next}})$ and $\tilde{u} \subseteq \mathcal{V}_{>t_{\text{next}}}$ (as the construction of \tilde{u}), we have:

$$\text{NOCT}(x'_o, o', u(x'_o, o')) = \min_{v \subseteq \mathcal{V}_{>t_{\text{next}}}} \text{NOCT}(x'_o, o', v) \leq \text{NOCT}(x'_o, o', \tilde{u}). \quad (16)$$

Combining Eq. (15) and Eq. (16) gives, for every realized $x_{a_{t_{\text{next}}}}$,

$$\mathcal{R}(x'_o, o', t_{\text{next}}) \leq \text{NOCT}(x'_o, o', \tilde{u}).$$

Taking the expectation over $\mathbb{E}_{x_{a_{t_{\text{next}}}} | x_o}$ preserves the inequality. Finally, substituting this bound into the decompositions of Eq. (12) and Eq. (13) (which share identical prefix terms up to t_{next}) yields:

$$\mathcal{R}(x_o, o, t) \leq \text{NOCT}(x_o, o, u(x_o, o)).$$

Hence, the results follow.

A.6. Future-Candidate Distribution ζ_o

In this section, we formally introduce the future-candidate distribution ζ_o . For any partially observed features x_o at time t and the corresponding labels y of the training dataset \mathcal{D} , we identify the top- κ candidate subsets $v_1, \dots, v_\kappa \subseteq \mathcal{V}_{>t} = \{(m, t') \mid m \in \{1, \dots, M\}, t' \in \{t+1, \dots, L\}\}$, in ascending order of the plug-in objective $\text{NOCT}_{\text{pl}}(x_o, o, v_l)$ (Eq. (3)). $\text{NOCT}_{\text{pl}}(x_o, o, v_l)$ quantifies the accuracy-cost tradeoff for candidate v_l , and we have access to x_{v_l} during training since x_{v_l} is from the training set. Now, each candidate v_l induces a uniform distribution ν_{v_l} over its selected feature-time pairs (and termination), defined as $\nu_{v_l}(m, t') = \frac{1}{|v_l|}$ if $(m, t') \in v_l$ and 0 otherwise. Intuitively, ν_{v_l} spreads equal probability mass over all acquisitions in the future candidate plan v_l . Note that in the case that v_l contains no further acquisition, $\nu_{v_l}(\emptyset) = 1$ (and if v_l is not empty $\nu_{v_l}(\emptyset) = 0$). The future-candidate distribution ζ_o for observed features x_o is the weighted sum of ν_{v_l} as

$$\zeta_o = \sum_{l=1}^{\kappa} w_l \nu_{v_l} \quad (17)$$

where $w_l = \frac{\exp(-\text{NOCT}_{\text{pl}}(x_o, o, v_l))}{\sum_{k=1}^{\kappa} \exp(-\text{NOCT}_{\text{pl}}(x_o, o, v_k))}$. Intuitively, given a partially observed feature x_o , ζ_o indicates how likely each feature at each timestep (and the termination) is chosen by weighting their accuracy-cost tradeoff. For each training sample $(x_i, y_i) \in \mathcal{D}$, we construct $\zeta_{i,o}$ accordingly.

A.7. Sensitivity Analysis

In this section, we provide further explanations of hyperparameters and how they affect performance. Overall, we find that our proposed method is robust to different settings, indicating that our method can be applied readily without excessive fine-tuning.

$|\mathcal{O}|$: this specifies the size of the candidate subset in our search. As $|\mathcal{O}|$ increases, NOCTA can explore a broader set of potential acquisition plans. As seen in Tab. 2 and Tab. 3, both estimators NOCT-Contrastive and NOCT-Amortized exhibit clear diminishing returns once $|\mathcal{O}|$ exceeds 1000.

κ : this controls how many top candidate subsets are aggregated to form the future acquisition distribution Eq. (17). Please refer to Tab. 5 for different settings.

K : this controls how many retrieved training samples in the learned embedding space are used to estimate future acquisition gains (Eq. 6). Small K can yield high-variance estimates due to limited support, while large K may include less similar samples. See Tab. 4 for different settings.

β : this controls the sensitivity that translates Jessen-Shannon divergence into a similarity score (Eq. 4). A larger β will penalize divergences more strongly, while a smaller β will be more lenient. Please refer to Tab. 6 for different settings.

γ : this determines the margin in the contrastive loss, making sure that dissimilar embeddings are pushed far apart (Eq. 5). If γ is too small, the embedding network might not push dissimilar pairs far enough, and if γ is too large, it might push moderately different samples by a large distance. Please refer to Tab. 7 for different settings.

Table 2. Ablation on the subset size $|\mathcal{O}|$ for NOCT-Contrastive used in the synthetic dataset

$ \mathcal{O} $	Accuracy	Cost
100	0.843 ± 0.001	13.252 ± 0.044
1000	0.855 ± 0.002	11.315 ± 0.012
5000	0.857 ± 0.001	12.046 ± 0.021
10000	0.857 ± 0.002	11.945 ± 0.012

 Table 3. Ablation on the subset size $|\mathcal{O}|$ for NOCT-Amortized used in the synthetic dataset

$ \mathcal{O} $	Accuracy	Cost
100	0.651 ± 0.010	11.401 ± 0.040
1000	0.666 ± 0.006	11.555 ± 0.087
5000	0.670 ± 0.016	11.430 ± 0.115
10000	0.664 ± 0.017	11.419 ± 0.150

 Table 4. Ablation on the number of retrieved instances K on the synthetic dataset.

K	Accuracy	Cost
5	0.815 ± 0.005	9.471 ± 0.033
10	0.801 ± 0.003	9.489 ± 0.006
25	0.816 ± 0.001	9.512 ± 0.006

 Table 5. Ablation on the number of top candidate subset κ used in the synthetic dataset

κ	Accuracy	Cost
5	0.815 ± 0.005	9.471 ± 0.033
10	0.814 ± 0.001	9.618 ± 0.022
25	0.811 ± 0.002	9.564 ± 0.067

 Table 6. Ablation on the scaling in similarity function β used in the synthetic dataset

β	Accuracy	Cost
0.5	0.810 ± 0.002	9.660 ± 0.054
1	0.815 ± 0.005	9.471 ± 0.033
2	0.821 ± 0.001	9.592 ± 0.022
5	0.819 ± 0.003	9.640 ± 0.048

 Table 7. Ablation on the margin in contrastive loss γ used in the synthetic dataset

γ	Accuracy	Cost
0.5	0.813 ± 0.010	9.592 ± 0.035
1	0.815 ± 0.005	9.471 ± 0.033
2	0.809 ± 0.005	9.638 ± 0.033
5	0.811 ± 0.001	9.688 ± 0.017

B. Experimental Setup

B.1. Cost of Features

Synthetic data. Our synthetic dataset includes 2 features, one being the digit and the other being the counter. Since both are generated through random selection, we assign an equal cost, 1, to the two features. Upon publication, we will release the synthetic dataset.

ADNI. The ADNI dataset includes 4 features per time point, with FDG and AV45 extracted from PET scans and Hippocampus and Entorhinal extracted from MRI scans. Since PET is a more expensive diagnosis, we follow Qin et al. (2024) and assign a cost 1 to FDG and AV45, and a cost 0.5 to Hippocampus and Entorhinal. Access to ADNI data may be requested via <https://adni.loni.usc.edu>, and the Data Use Agreement is available at <https://adni.loni.usc.edu/terms-of-use/>.

OAI. We use a total of 27 features for the OAI dataset, with 17 clinical measurements, and 10 joint space width (JSW) extracted from knee radiography. For the clinical measurements, we assign a low cost of 0.3 to those that require minimum effort, e.g., age, sex, and race, and a slightly higher cost of 0.5 to blood pressure and BMI calculation. For JSW, a cost of 1.0 is assigned for the minimum JSW and 0.8 for those measured at different positions. Access to the OAI data may be requested via <https://nda.nih.gov/oai/>.

B.2. Baseline Implementation

For ASAC, RAS, and AS, we use the implementation available at https://github.com/yvchao/cvar_sensing, which is under the BSD-3-Clause license. For DIME (Gadgil et al., 2024), we extend the method to longitudinal by building on top of the official implementation available at <https://github.com/suinleelab/DIME>. The DiFA codebase is not publicly released, and researchers may request it directly from the authors.

Following Qin et al. (2024), we share the same neural CDE predictor (Kidger et al., 2020) for ASAC, RAS, and AS. Following the authors' released code, we treat the drop rate p of the auxiliary observation strategy π_0 (the same notation as in Qin et al. (2024)) as a hyperparameter and sweep $p \in \{0.0, 0.3, 0.5, 0.7\}$. We select p based on the outcome predictor's average accuracy over five randomly masked test sets generated by π_0 . This matches the original evaluation protocol to ensure comparability and reproducibility. The selected drop rates are $p = 0.3$ (Synthetic), $p = 0.7$ (ADNI), $p = 0.5$ (WOMAC), and $p = 0.3$ (KLG).

ASAC (Yoon et al., 2019). We select the coefficient for the acquisition cost: 1) $\mu \in \{0.0015, 0.002, 0.003\}$ for the synthetic dataset, 2) $\mu \in \{0.005, 0.02\}$ for ADNI, 3) $\mu \in \{0.0012, 0.0016, 0.003\}$ for the WOMAC of OAI dataset, and 4) $\mu \in \{0.00125, 0.0015, 0.00175, 0.005\}$ for the KLG of OAI dataset. Note that we report multiple final μ because we evaluate ASAC across multiple acquisition costs.

RAS (Qin et al., 2024). For the synthetic dataset, we set the allowed acquisition interval to $(\Delta_{\min} = 0.2, \Delta_{\max} = 1.0)$ for the synthetic dataset, $(\Delta_{\min} = 0.5, \Delta_{\max} = 1.5)$ for ADNI, and $(\Delta_{\min} = 0.5, \Delta_{\max} = 4.5)$ for WOMAC and KLG.

Moreover, for RAS we tune the diagnostic-error coefficient γ^{RAS} on the validation set via a grid search. Specifically, we sweep $\gamma^{\text{RAS}} \in \{200, 250, 280, 300, 310, 320, 350, 400, 5000, 7000, 9000\}$ (Synthetic), $\{50, 75, 100, 175, 200, 250, 300, 350, 400, 450\}$ (ADNI), $\{200, 250, 300, 350, 400, 450, 2000, 3000, 4500, 9000\}$ (WOMAC), and $\{200, 250, 300, 350, 400, 450, 1200, 1700\}$ (KLG), and select the best value per dataset. The final selected values are $\gamma^{\text{RAS}} \in \{5000, 7000, 9000\}$ (Synthetic), $\{50, 75, 100, 175\}$ (ADNI), $\{2000, 4500, 9000\}$ (WOMAC), and $\{1200, 1700\}$ (KLG); we report multiple final γ^{RAS} because we evaluate RAS across multiple acquisition costs. For all datasets, we use a tail-risk quantile of 0.1, an invalid-visit penalty of 10, and a discount factor of 0.99, following the authors' defaults.

AS (Qin et al., 2024). We set the minimum and maximum allowed acquisition intervals as in the RAS setting. In addition, we select fixed acquisition interval of: 1) $\tilde{\Delta} \in \{0.2, 0.4\}$ for the synthetic dataset, 2) $\tilde{\Delta} \in \{0.5, 1.0, 1.5\}$ for ADNI dataset, 3) $\tilde{\Delta} \in \{0.5, 1.5\}$ for WOMAC of OAI, and 4) $\tilde{\Delta} \in \{0.5, 1.5\}$ for KLG of OAI dataset. Note that we report multiple final $\tilde{\Delta}$ because we evaluate AS across multiple acquisition costs.

DIME (Gadgil et al., 2024). For this baseline, we extend the original model to the longitudinal setting, while still keeping its greedy feature acquisition strategy. Both the prediction network and value network of DIME share the same architecture as our NOCTA–Amortized model, and hence we use the same training strategies.

DiFA (Ghosh and Lan, 2023). Following Ghosh and Lan (2023), we use a variational autoencoder with arbitrary conditioning (VAEAC) probabilistic model (Ivanov et al., 2019) for imputation. When using the same architecture with NOCT-Contrastive, DiFA performs poorly. Hence, we gave DiFA an advantage and used the recommended architecture from the DiFA paper. That is, both the prediction network and the feature policy model have two fully connected layers (hidden size 128) with skip connections, dropout regularizer, and LeakyReLU activation function.

B.3. NOCTA Implementation

Prediction Network. We share the same MLP architecture for both NOCT-Contrastive and NOCT-Amortized. Specifically, the network consists of two hidden layers with ReLU. Each hidden layer contains 10 units for the synthetic and ADNI datasets, and 32 units for the WOMAC and KLG of the OAI dataset, respectively. Moreover, we apply random dropout for the input during training of the predictor.

NOCT-Contrastive. We select the accuracy-cost trade-off hyperparameter: 1) $\alpha \in \{0.002, 0.006, 0.02, 0.03\}$ for the synthetic dataset, 2) $\alpha \in \{0.003, 0.005, 0.01\}$ for ADNI dataset, 3) $\alpha \in \{0.00075, 0.005, 0.01\}$ for WOMAC of OAI dataset, and 4) $\alpha \in \{0.0025, 0.001, 0.006\}$ for KLG of OAI dataset.

For the embedding network, we use four hidden layers with ReLU. Each hidden layer contains 32 units for the synthetic and ADNI datasets, and 64 units for the WOMAC and KLG of the OAI dataset, respectively.

NOCT-Amortized. For the estimator f_θ , we use an MLP architecture with two hidden layers and ReLU as the activation function. We use the same hidden size as the prediction network, but the number of outputs is set to be 1 for estimating the utility of the potential subset. We set the accuracy-cost trade-off hyperparameter α to $5e-5$ for WOMAC and $5e-4$ for all other tasks, and the acquisition terminates by either selecting the empty set or reaching the budget.

To promote more stable training for Eq. (9) in NOCT-Amortized, we slightly modify the neural network estimator f_θ 's target in two ways. First, instead of regressing to the full plug-in objective Eq. (3), we train the estimator f_θ to predict only the predictive-loss:

$$\widetilde{\text{NOCT}}_{\text{pl}}(x_o, o, v) \triangleq \ell(x_o \cup x_v, y, t), \quad (18)$$

and add $\alpha \sum_{(m, t') \in v} c^m$ explicitly when ranking candidate plans, since it depends only on v (which we have access to during inference time). Second, we further reformulate the target as the gain relative to terminating with the current information:

$$\Delta_{\text{pl}}(x_o, o, v) \triangleq \ell(x_o, y, t) - \widetilde{\text{NOCT}}_{\text{pl}}(x_o, o, v). \quad (19)$$

Because $\ell(x_o, y, t)$ is constant w.r.t. v at a fixed state (x_o, o, t) , maximizing Δ_{pl} is equivalent to minimizing $\widetilde{\text{NOCT}}_{\text{pl}}$ (and thus yields the same plan $u(x_o, o)$ in Eq. (2)). That is, the target of the neural network estimator f_θ is now $\Delta_{\text{pl}}(x_o, o, v)$, and this implicitly normalizes the target scale.

B.4. Hardware

We employed two different clusters for our experiments: (1) Intel Xeon CPU E5-2630 v4 and NVIDIA GeForce GTX 1080 for experiments, and (2) Intel Xeon Silver 4114 CPU and NVIDIA GeForce GTX 2080. We used cluster (1) for RAS, AS, ASAC, DiFA, NOCT-Contrastive, and cluster (2) for DIME and NOCT-Amortized.

C. Additional Results

C.1. ROC AUC on Real-World Datasets

Following Qin et al. (2024), Fig. 5 shows additional ROC AUC results on real-world datasets across varying average acquisition budgets. Our method consistently outperforms all baselines while using a lower cost.

C.2. Full Results with Mean and Standard Deviation

Tables. 8, 9, 10, and 11 report the mean and standard deviation for each data point presented in Figs. 3 and 5, computed over five independent runs.

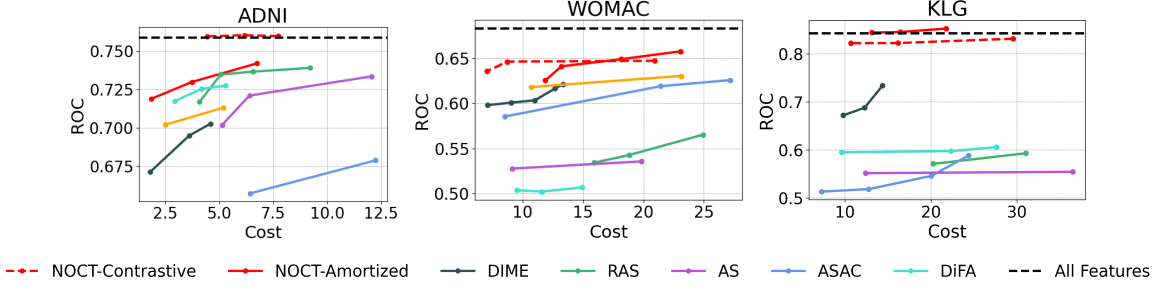


Figure 5. Additional results on performance/cost of models, measured by ROC AUC across varying average acquisition budgets on real-world datasets. Best viewed in color.

Table 8. Full results for accuracy vs. average cost on synthetic dataset.

METHOD	SYNTHETIC	
	ACCURACY	COST
ASAC	0.449 \pm 0.078	5.803 \pm 5.180
	0.567 \pm 0.161	9.929 \pm 8.365
	0.624 \pm 0.136	11.780 \pm 5.211
RAS	0.316 \pm 0.031	6.390 \pm 5.316
	0.315 \pm 0.032	6.852 \pm 5.129
	0.336 \pm 0.022	11.003 \pm 2.638
AS	0.320 \pm 0.014	9.210 \pm 2.344
	0.335 \pm 0.033	12.870 \pm 3.762
DIME	0.497 \pm 0.078	4.000 \pm 0.000
	0.501 \pm 0.080	4.662 \pm 0.557
	0.509 \pm 0.084	5.375 \pm 1.213
DiFA	0.444 \pm 0.015	6.466 \pm 0.058
	0.463 \pm 0.017	8.249 \pm 0.420
	0.504 \pm 0.010	10.138 \pm 0.129
NOCT-CONTRASTIVE	0.670 \pm 0.002	6.494 \pm 0.005
	0.815 \pm 0.005	9.471 \pm 0.033
	0.855 \pm 0.002	11.315 \pm 0.012
NOCT-AMORTIZED	0.512 \pm 0.018	3.580 \pm 0.292
	0.603 \pm 0.026	6.906 \pm 0.174
	0.640 \pm 0.017	8.6358 \pm 0.164
	0.666 \pm 0.006	11.555 \pm 0.087

Table 9. Full results for AP and ROC vs. average cost on ADNI prediction.

METHOD	ADNI		
	AP	ROC	COST
ASAC	0.449 \pm 0.041	0.657 \pm 0.038	6.442 \pm 6.093
	0.497 \pm 0.034	0.679 \pm 0.015	12.242 \pm 2.648
RAS	0.538 \pm 0.036	0.717 \pm 0.024	4.087 \pm 0.735
	0.567 \pm 0.015	0.735 \pm 0.008	5.064 \pm 0.324
	0.567 \pm 0.022	0.737 \pm 0.012	6.560 \pm 2.459
AS	0.572 \pm 0.012	0.739 \pm 0.011	9.197 \pm 1.438
	0.514 \pm 0.046	0.702 \pm 0.038	5.133 \pm 1.659
	0.536 \pm 0.021	0.721 \pm 0.014	6.394 \pm 2.477
DIME	0.546 \pm 0.021	0.734 \pm 0.013	12.054 \pm 1.763
	0.519 \pm 0.037	0.671 \pm 0.047	1.801 \pm 0.050
	0.538 \pm 0.045	0.695 \pm 0.048	3.607 \pm 0.084
DiFA	0.544 \pm 0.048	0.703 \pm 0.049	4.587 \pm 0.330
	0.520 \pm 0.027	0.717 \pm 0.029	2.925 \pm 0.127
	0.529 \pm 0.025	0.725 \pm 0.028	4.180 \pm 0.043
NOCT-CONTRASTIVE	0.530 \pm 0.027	0.727 \pm 0.033	5.292 \pm 0.107
	0.578 \pm 0.004	0.760 \pm 0.003	4.434 \pm 0.042
	0.579 \pm 0.009	0.760 \pm 0.003	6.164 \pm 0.068
NOCT-AMORTIZED	0.584 \pm 0.013	0.760 \pm 0.006	7.727 \pm 0.094
	0.548 \pm 0.025	0.719 \pm 0.025	1.851 \pm 0.019
	0.569 \pm 0.023	0.730 \pm 0.015	3.729 \pm 0.079
	0.576 \pm 0.021	0.742 \pm 0.012	6.743 \pm 0.330

Table 10. Full results for AP and ROC vs. average cost on WOMAC score prediction.

METHOD	WOMAC		
	AP	ROC	COST
ASAC	0.269 \pm 0.032	0.586 \pm 0.060	8.541 \pm 2.136
	0.293 \pm 0.018	0.619 \pm 0.028	21.423 \pm 6.480
RAS	0.299 \pm 0.025	0.626 \pm 0.026	27.175 \pm 6.933
	0.226 \pm 0.008	0.534 \pm 0.019	15.930 \pm 3.475
	0.231 \pm 0.007	0.543 \pm 0.009	18.810 \pm 1.802
AS	0.251 \pm 0.019	0.565 \pm 0.024	24.939 \pm 3.796
	0.225 \pm 0.005	0.528 \pm 0.008	9.160 \pm 2.271
	0.235 \pm 0.011	0.536 \pm 0.012	19.826 \pm 10.326
DIME	0.297 \pm 0.025	0.598 \pm 0.043	7.073 \pm 0.093
	0.297 \pm 0.025	0.601 \pm 0.043	9.036 \pm 0.198
	0.302 \pm 0.028	0.603 \pm 0.044	11.009 \pm 0.310
DiFA	0.305 \pm 0.027	0.617 \pm 0.037	12.696 \pm 0.357
	0.310 \pm 0.028	0.621 \pm 0.038	13.325 \pm 0.643
	0.199 \pm 0.009	0.504 \pm 0.004	9.532 \pm 0.091
NOCT-CONTRASTIVE	0.211 \pm 0.005	0.502 \pm 0.002	11.584 \pm 0.630
	0.217 \pm 0.004	0.507 \pm 0.008	14.936 \pm 1.433
	0.317 \pm 0.003	0.636 \pm 0.0012	7.063 \pm 0.004
NOCT-AMORTIZED	0.328 \pm 0.004	0.646 \pm 0.003	8.729 \pm 0.011
	0.339 \pm 0.008	0.647 \pm 0.003	20.921 \pm 0.058
	0.311 \pm 0.007	0.625 \pm 0.006	11.862 \pm 0.074
	0.327 \pm 0.020	0.641 \pm 0.018	13.212 \pm 0.180
	0.335 \pm 0.015	0.649 \pm 0.015	18.178 \pm 0.082
	0.340 \pm 0.013	0.658 \pm 0.011	23.061 \pm 0.059

Table 11. Full results for AP and ROC vs. average cost on KLG prediction.

METHOD	KLG		
	AP	ROC	COST
ASAC	0.258 \pm 0.021	0.513 \pm 0.035	7.284 \pm 4.694
	0.266 \pm 0.018	0.519 \pm 0.019	12.756 \pm 6.584
	0.283 \pm 0.009	0.546 \pm 0.024	20.025 \pm 6.504
	0.304 \pm 0.008	0.589 \pm 0.015	24.361 \pm 15.940
RAS	0.290 \pm 0.012	0.571 \pm 0.023	20.253 \pm 11.269
	0.313 \pm 0.049	0.593 \pm 0.063	31.044 \pm 8.560
AS	0.277 \pm 0.012	0.552 \pm 0.021	12.394 \pm 2.027
	0.285 \pm 0.022	0.555 \pm 0.015	36.499 \pm 8.124
DIME	0.418 \pm 0.016	0.672 \pm 0.023	9.787 \pm 0.040
	0.438 \pm 0.018	0.688 \pm 0.028	12.281 \pm 0.005
	0.486 \pm 0.026	0.734 \pm 0.024	14.359 \pm 0.148
DiFA	0.310 \pm 0.006	0.595 \pm 0.019	9.611 \pm 1.743
	0.322 \pm 0.011	0.598 \pm 0.015	22.331 \pm 3.465
	0.336 \pm 0.010	0.606 \pm 0.013	27.615 \pm 6.411
NOCT-CONTRASTIVE	0.644 \pm 0.003	0.822 \pm 0.001	10.687 \pm 0.018
	0.649 \pm 0.002	0.822 \pm 0.002	16.192 \pm 0.062
	0.663 \pm 0.004	0.831 \pm 0.001	29.546 \pm 0.052
NOCT-AMORTIZED	0.641 \pm 0.054	0.844 \pm 0.020	13.144 \pm 0.107
	0.639 \pm 0.056	0.845 \pm 0.022	16.448 \pm 0.228
	0.655 \pm 0.042	0.853 \pm 0.017	21.776 \pm 0.323